

Graphical Abstract

Bayesian Optimisation using microscopic and integral measurements to infer nuclear data parameters

Daan Houben, Mathieu Hursin, Luca Fiorito, Pierre-Etienne Labeau, Gert Van den Eynde

Highlights

Bayesian Optimisation using microscopic and integral measurements to infer nuclear data parameters

Daan Houben, Mathieu Hursin, Luca Fiorito, Pierre-Etienne Labeau, Gert Van den Eynde

- Research highlight 1
- Research highlight 2

Bayesian Optimisation using microscopic and integral measurements to infer nuclear data parameters

Daan Houben^{a,b,c}, Mathieu Hursin^c, Luca Fiorito^a, Pierre-Etienne Labeau^b, Gert Van den Eynde^a

^aThe Belgian Nuclear Research Center (SCK CEN), Boeretang 190, Mol, 2400, Antwerp, Belgium

^bUniversité Libre de Bruxelles (ULB), Av. Franklin Roosevelt 50, Bruxelles, 1050, Bruxelles, Belgium

^cÉcole Polytechnique Fédérale de Lausanne (EPFL), Rte Cantonale, Lausanne, 1015, Vaud, Switzerland

Abstract

Abstract text.

Keywords: Nuclear data, MCMC, data assimilation, Chromium

1. Introduction

Nuclear data is considered the major source of uncertainty in several reactor observables, most notably the effective multiplication factor (k_{eff}). The nuclear data available in evaluated nuclear data libraries—such as cross sections, neutron multiplicities, angular distributions, and fission neutron energy spectra—are the result of a complex fitting procedure involving theoretical models, microscopic experiments, and expert judgment. Integral experiments are subsequently used to assess the performance of this nuclear data. In this work, a Bayesian Optimization (BO) framework is proposed to consolidate microscopic energy-dependent measurements with integral experiments for the estimation of nuclear data parameters.

The BO is performed using a Markov Chain Monte Carlo (MCMC) method, in which surrogates are employed to evaluate the likelihoods. For the microscopic energy-dependent measurements, the SAMMY v8.1.0 resonance fitting tool [1] is employed, while SERPENT v2.2.2 [2], a Monte Carlo neutron transport code, is used to quantify the integral response. Surrogates are trained by evaluating random samples drawn in the input space using these high-fidelity models. The methodology is tested on a case study involving ^{53}Cr . Since microscopic experiments typically provide a dense set of data points while integral experiments provide a single values integrated over several nuclides/reactions/energies, special care is taken to analyze how different assumptions regarding the likelihood evaluation and data correlation affect the posterior distribution.

17 2. Background and Mathematical Motivation

18 2.1. Bayesian Optimization Setup

The main objective of this paper is to infer nuclear data parameter(s) from a combined set of microscopic energy-dependent and integral experiments. Microscopic energy-dependent measurements (hereafter referred to as microscopic measurements) quantify single-energy neutron properties. These often result from neutron Time-Of-Flight (nTOF) facilities, where the neutron energy is derived from the time of flight to a target. A characteristic of these measurements is the high density of data points obtained. In contrast, integral measurements, such as criticality experiments, provide a single value representative of a macroscopic group of nuclides, reactions, and energies.

According to Bayes' theorem, the posterior (updated) probability density function (PDF), $P(\theta|\text{data})$, is proportional to the likelihood of observing the parameter(s) θ given the data, multiplied by the prior belief regarding the parameter(s):

$$P(\theta|\text{data}) \propto P(\text{data}|\theta) \cdot P(\theta) \quad (1)$$

For brevity, we refer to the likelihood as $\mathcal{L}(\theta) = P(\text{data}|\theta)$.

Email address: daan.houben@sckcen.be (Daan Houben)

29 2.2. Markov Chain Monte Carlo (MCMC)

30 To calculate the posterior distribution, various techniques derived from Bayes' theorem can be employed, such as
 31 Generalized Linear Least Squares (GLLS) [3], Bayesian Monte Carlo (BMC) [4], and MOCABA [5]. In this paper,
 32 we select an algorithm belonging to the family of Markov Chain Monte Carlo (MCMC) techniques.

33 In most MCMC algorithms, the unnormalized posterior is evaluated for each sample as

$$P^*(\theta|\text{data}) = \mathcal{L}(\theta) \cdot P(\theta), \quad (2)$$

34 where $P^*(\theta|\text{data})$ represents the posterior up to a normalizing constant. The objective is to construct a Markov chain
 35 $\{\theta_0, \theta_1, \dots, \theta_N\}$ such that the stationary distribution of the chain converges to the posterior distribution $P(\theta|\text{data})$. Under
 36 the assumption of a Normally distributed prior ($\mathcal{N}(\theta_0, \Sigma)$) and likelihood ($\mathcal{N}(\mathbf{y}_{\text{true}}, \mathbf{A})$), the unnormalized posterior
 37 probability evaluated at θ can be rewritten as

$$\begin{aligned} P^*(\theta|\text{data}) &= \frac{1}{\sqrt{(2\pi)^m \det \mathbf{A}}} \exp \left[-\frac{1}{2} (\mathbf{f}(\theta) - \mathbf{y}_{\text{exp}})^T \mathbf{A}^{-1} (\mathbf{f}(\theta) - \mathbf{y}_{\text{exp}}) \right] \times \\ &\quad \frac{1}{\sqrt{(2\pi)^n \det \Sigma}} \exp \left[-\frac{1}{2} (\theta_0 - \theta)^T \Sigma^{-1} (\theta_0 - \theta) \right] \end{aligned} \quad (3)$$

38 The first term represents the probability of observing θ given the measurements, where \mathbf{y}_{exp} is the vector describing
 39 the m measurement points, $\mathbf{f}(\theta)$ is the vector containing the model responses for the vector θ , and \mathbf{A} is the covariance
 40 matrix describing the measurement points of size ($m \times m$). The prior probability is calculated using the prior belief of
 41 the n parameters θ_0 , with a covariance matrix Σ of size ($n \times n$).

42 Standard algorithms, such as Metropolis-Hastings, propose a new state θ' based on a proposal distribution $q(\theta'|\theta_i)$
 43 and accept it with probability α . However, as Metropolis-Hastings algorithms require tuning, we employ the Affine
 44 Invariant Ensemble Sampler (AIES), as implemented in the *emcee* code [6]. In this algorithm, an ensemble of K
 45 "walkers" is propagated in parallel. The proposal step for a walker θ_k is based on the current position of a comple-
 46 mentary walker θ_j from the ensemble:

$$\theta'_k = \theta_j + Z(\theta_k - \theta_j) \quad (4)$$

47 where Z is a scaling variable drawn from a distribution $g(z) \propto 1/\sqrt{z}$ on the interval $[1/a, a]$. This "stretch move"
 48 allows the algorithm to efficiently sample distributions with strong correlations without requiring manual tuning of
 49 the proposal covariance matrix.

50 2.3. Likelihood Formulation

51 The formulation of the likelihood function $\mathcal{L}(\theta)$ is one of the challenges when combining integral and microscopic
 52 data. The quantity of data points differs by orders of magnitude, which may dilute the effect of the integral measure-
 53 ment. To better understand the extent to which microscopic measurements might dilute these integral measurements,
 54 we analyze different approaches to include the microscopic experiments.

55 Ideally, one would use the full experimental covariance matrix. However, calculating experimental correlations
 56 between distinct integral experiments, distinct microscopic, and between microscopic and integral experiments, is
 57 inherently difficult and time consuming. We therefore currently introduce the assumption that there are no corre-
 58 lations between microscopic and integral experiments, nor between integral or microscopic experiments from different
 59 facilities. This allows us to calculate the total likelihood $\mathcal{L}(\theta)$ for a set of microscopic experiments J and integral
 60 experiments I :

$$\begin{aligned} \mathcal{L}(\theta) &= \prod_{j \in J} \frac{1}{\sqrt{(2\pi)^{m_j} \det \mathbf{A}_j}} \exp \left[-\frac{1}{2} (\mathbf{f}_j(\theta) - \mathbf{y}_j)^T \mathbf{A}_j^{-1} (\mathbf{f}_j(\theta) - \mathbf{y}_j) \right] \times \\ &\quad \prod_{i \in I} \frac{1}{\sqrt{2\pi\sigma_i^2}} \exp \left[-\frac{(f_i(\theta) - y_i)^2}{2\sigma_i^2} \right] \end{aligned} \quad (5)$$

61 Using the log-likelihood $\ln \mathcal{L}(\theta)$ for numerical stability:

$$\begin{aligned}\ln \mathcal{L}(\theta) = & -\frac{1}{2} \sum_{j \in J} \ln [(2\pi)^{m_j} \det \mathbf{A}_j] - \frac{1}{2} \sum_{j \in J} [(\mathbf{f}_j(\theta) - \mathbf{y}_j)^T \mathbf{A}_j^{-1} (\mathbf{f}_j(\theta) - \mathbf{y}_j)] + \\ & -\frac{1}{2} \sum_{i \in I} \ln [2\pi\sigma_i^2] - \frac{1}{2} \sum_{i \in I} \frac{(f_i(\theta) - y_i)^2}{\sigma_i^2}\end{aligned}\quad (6)$$

62 We analyze two approximations regarding the microscopic data: (1) all microscopic measurement points behave fully
63 independently, and (2) microscopic points within a single experiment are fully correlated (correlation coefficient of 1)
64 while remaining independent of other experiments.

65 2.3.1. Independent microscopic measurement points

66 If all measurement points are independent, each microscopic point carries the same weight as an integral experi-
67 ment. Consequently, the integral experiments are likely to be diluted and their influence on the posterior negligible.
68 This makes the inference overconfident in the microscopic experiments. The log-likelihood from Eq. 6 becomes:

$$\begin{aligned}\ln \mathcal{L}_J(\theta) = & -\frac{1}{2} \sum_{j \in J} \sum_{e \in E_j} \ln [2\pi\sigma_{j,e}^2] - \frac{1}{2} \sum_{j \in J} \sum_{e \in E_j} \left[\frac{(f_{j,e}(\theta) - y_{j,e})^2}{\sigma_{j,e}^2} \right] \\ & = C - \frac{1}{2} \sum_{j \in J} \chi_j^2\end{aligned}\quad (7)$$

69 where χ^2 is the standard goodness-of-fit. The logarithmic term is constant with respect to θ and is replaced by C .

70 2.3.2. Fully correlated microscopic measurement points

71 Conversely, if we assume microscopic points are fully correlated, we normalize by the degrees of freedom (N),
72 which may be interpreted as taking the average. Eq. 6 then becomes

$$\begin{aligned}\ln \mathcal{L}_J(\theta) = & -\frac{1}{2} \sum_{j \in J} \frac{1}{N} \sum_{e \in E_j} \ln [2\pi\sigma_{j,e}^2] - \frac{1}{2} \sum_{j \in J} \frac{1}{N} \sum_{e \in E_j} \left[\frac{(f_{j,e}(\theta) - y_{j,e})^2}{\sigma_{j,e}^2} \right] \\ & = C - \frac{1}{2} \sum_{j \in J} \chi_{N,j}^2,\end{aligned}\quad (8)$$

73 where $\chi_{N,j}^2$ is the chi-squared per degree of freedom for microscopic experiment j . In this approximation, we are
74 too conservative and do not trust the microscopic experiment sufficiently. Eventually, including the full experimental
75 covariance matrix will result in a likelihood which is a combination of Eqs. 7 and 8.

76 2.4. Surrogate Modelling

77 The MCMC algorithm requires thousands of likelihood evaluations. Directly executing high-fidelity codes (SAMMY
78 and SERPENT) at each step is computationally expensive. We therefore employ Gaussian Process (GP) regression
79 as a surrogate model. A GP defines a probability distribution over all possible functions consistent with the observed
80 data, providing both a predicted mean and an associated variance. This variance can then be included in the likelihood
81 calculation and allows the MCMC sampler to avoid overconfidence in less explored regions of the input space.

82 To train the surrogates, a dataset is generated by drawing uniform random samples across the input space. For
83 microscopic experiments, SAMMY calculates the χ^2 metric. For integral experiments, SERPENT calculates k_{eff} .
84 The dataset is split 80/20 for training and testing. We utilize a Radial Basis Function (RBF) kernel for the integral
85 experiments (as k_{eff} behaves smoothly) and a polynomial kernel of second degree for the microscopic χ^2 response (as
86 χ^2 is inherently quadratic). A white noise kernel is added to account for Monte Carlo statistical uncertainty and to
87 ensure positive definiteness.

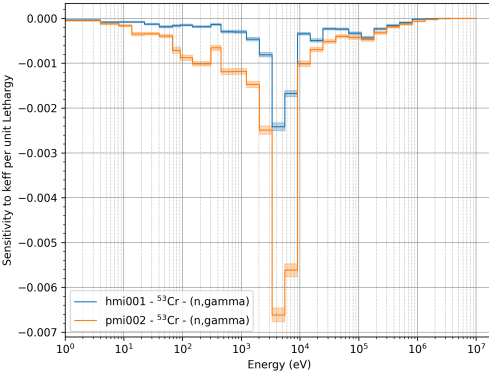


Figure 1: Sensitivity profiles for two criticality experiments sensitive to Cr-53 (n,γ)

88 2.5. Including Uncertainties of Other Nuclides

89 To limit the Bayesian Optimization from compensating for biases induced by other sources, next to the uncertainties
90 introduced by material and geometry specifications, uncertainties from other nuclides should also be included.
91 For criticality experiments, we estimate these using relative first-order sensitivity coefficients $S_{k,\sigma} = \frac{\partial k/k}{\partial \sigma \sigma}$ calculated
92 via Generalized Perturbation Theory (GPT) as implemented in SERPENT-2 using the ECCO-33 multi-group energy
93 structure [7].

94 Covariance matrices Σ_σ were generated using SANDY [8] (wrapping NJOY2016 [9]). The Sandwich formula
95 [10] is used to propagate these uncertainties to k_{eff} , it is given by

$$\Sigma_k = S_{k,\sigma}^T \cdot \Sigma_\sigma \cdot S_{k,\sigma}, \quad (9)$$

96 where Σ_k is the covariance matrix describing k_{eff} of the systems under consideration and $S_{k,\sigma}$, the matrix containing
97 the sensitivity vectors of each system, is the relative first-order sensitivity coefficients describing how changes in
98 nuclear data affect k_{eff} . This additional nuclear data variance is added to the experimental variance. This ensures the
99 adjustment does not falsely correct for other nuclear data biases. As a consequence, the integral experiments (mostly
100 criticality) become less informative, as they are heavily influenced by uncertainties due to fissile nuclides.

101 3. Description of Cases

102 3.1. Chromium-53

103 Chromium is a frequently used structural element in nuclear reactors, here 11-26% of chromium is added to
104 stainless steel in order to increase its corrosion resistance. Due to the scattering and capture cross sections in ^{50}Cr ,
105 ^{52}Cr and ^{53}Cr , it is also important for criticality safety in some nuclear systems [11]. A major isotope with relatively
106 poor nuclear data is the 1-10 keV range of ^{53}Cr . Existing microscopic measurements, such as those by Guber (2011)
107 [12] and Stieglitz (1971) [13], are not consistent with each other. Recently, Pérez-Maroto et al. (2025) performed
108 new capture yield measurements, it is seen as a possibility to include this experiment and complement it with integral
109 experiments to test the proposed methodology.

110 To start, we selected two criticality experiments, i.e., PMI-002 and HMI-001, due to their significant sensitivity
111 in the 1-10 keV range (see Figure 1). These experiments use stainless steel as reflector in an intermediate spectrum.
112 They are available in the International Handbook of Evaluated Criticality Safety Benchmark Experiments (ICSBEP)
113 [14].

114 For this case study, we infer only the capture width Γ_γ at 4 keV, as it is the parameter most sensitive to criticality in
115 this range. E_r and Γ_n are not perturbed as they are more easily derived from transmission measurements. This serves
116 as a simplified proof-of-concept and an extension to multiple input parameters is possible. The perturbation of Γ_γ is
117 shown in Figure 2. Here, the capture yield (a) represents the connection to the microscopic measurements performed
118 by Pérez-Maroto et al., while (b) represents the cross sections which have been incorporated into ACE files, ready for
119 use in the SERPENT-2 Monte Carlo code. For each of these curves, the SAMMY and SERPENT codes were run with
120 the goal of training a surrogate GP.

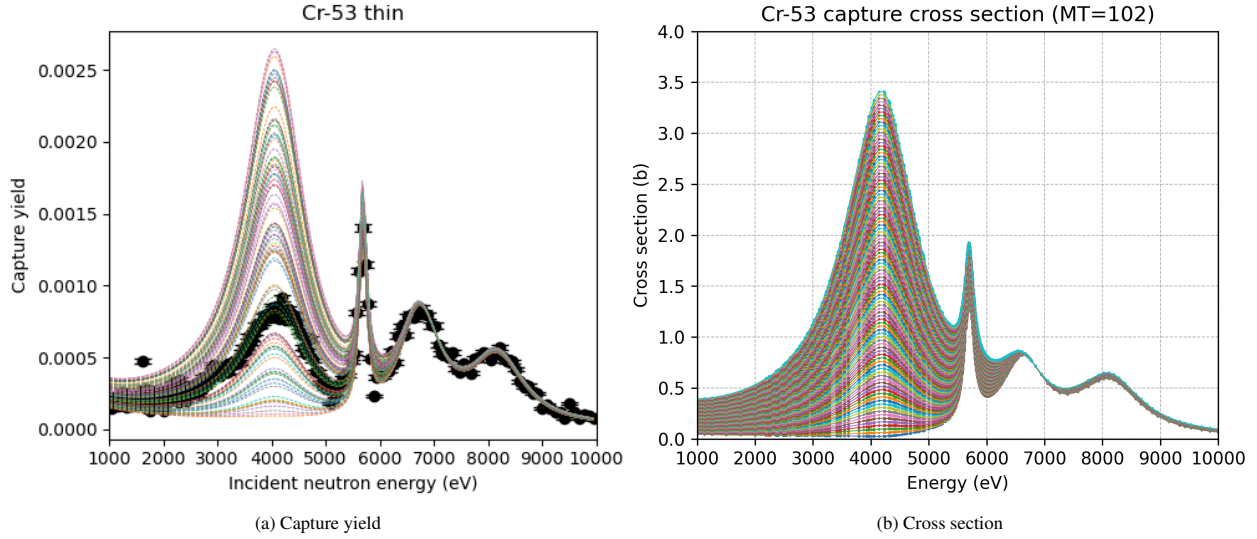


Figure 2: Random samples for capture yield (A) and cross section (B).

Table 1: Overview of posterior mean and uncertainty for different combinations of experiments included.

Case	PMI002	HMI001	ntof	Γ_γ, eV	$\sigma_\Gamma (\%)$	Comment
1				4.14	20	Prior
2	✓	✓		4.16	19.7	
3			✓	3.14	6	
4	✓	✓	✓	3.15	6	Fully correlated
5	✓	✓	✓	3.09	2	Independent
6	✓	✓		5.52	13	No other ND uncertainty
7			✓	3.09	2	Independent

4. Results and Discussions

4.1. Chromium-53

The validation of the Gaussian Process is shown in Figure 3, in (a) the data points and the GP for the Pérez-Maroto data set is shown, while in (b) it is shown for PMI-002. The GP corresponds well with the predicted responses obtained from SAMMY and SERPENT, obviously since they were trained on them. Nevertheless, the tests performed on the 20% of data points which were not included in the assimilation were also in good agreement with the GP prediction.

We analyze several scenarios: integral experiments only, microscopic experiments only, and combinations using the independent vs. fully correlated assumptions. The results are summarized in Table 1.

To confine the effect of including some experiments, various scenarios are simulated. In case 1, no experiments are included, which corresponds to the prior input parameters taken from JEFF-4.0, but with an increased relative uncertainty to make the prior less informative. Then, as a baseline Eq. 8 is used unless otherwise noted. In case 2, both integral experiments are included and the mean shifts only slightly and the posterior uncertainty is also not improved much. This can be attributed to the large uncertainty due to other nuclear data uncertainties in comparison to the rather limited sensitivity to the first Γ_γ of ^{53}Cr . In contrast, when these other nuclear data uncertainties are neglected, as can be seen in case 6, the bias shifts by about 30%, while the uncertainty is reduced by 7%.

Now, the influence of fully correlated and independent microscopic measurement points is compared. In case 3, only the microscopic experiment from Pérez-Maroto is included with the assumption of fully correlated measurement points. Then, the posterior is optimized to be consistent with only this measurement and the Γ_γ moves down. This is in contradiction with the adjustment proposed by case 6, but cannot be rejected by the posterior in case 2 where the other nuclear data uncertainties are included. The posterior uncertainty is then reduced to 6%. Now, when the assumption

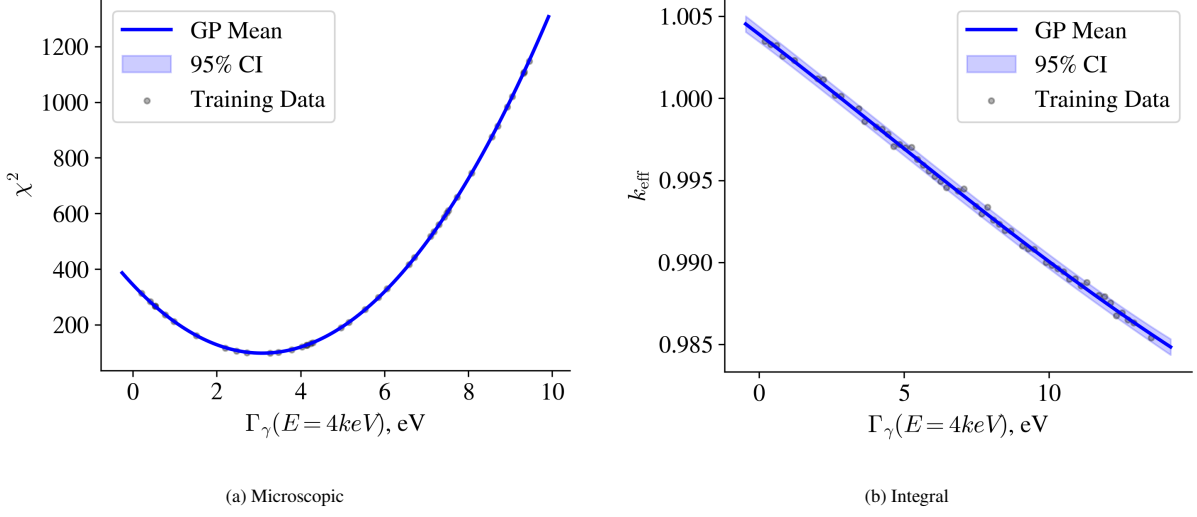


Figure 3: GPs for microscopic (a) and integral (b) experiment.

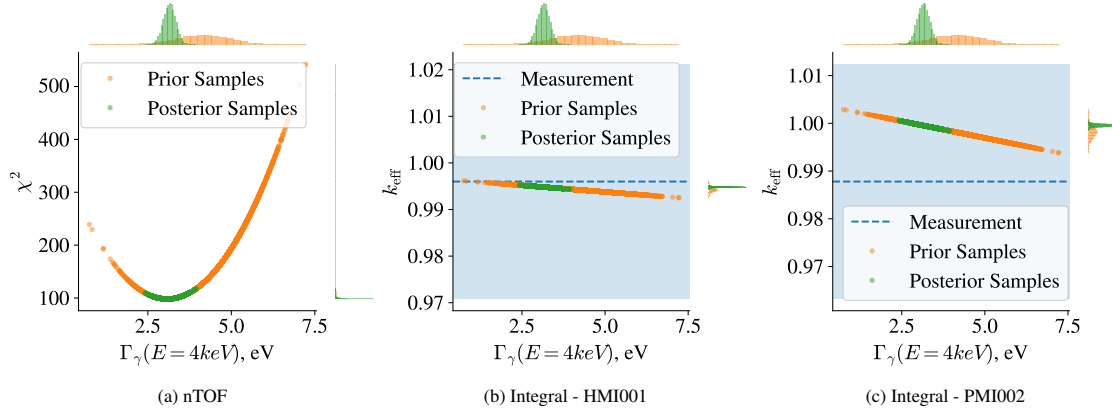


Figure 4: Scatter plots for microscopic (A) and integral (B and C) experiments showing the prior and posterior responses as a function of the input variable for Case 4.

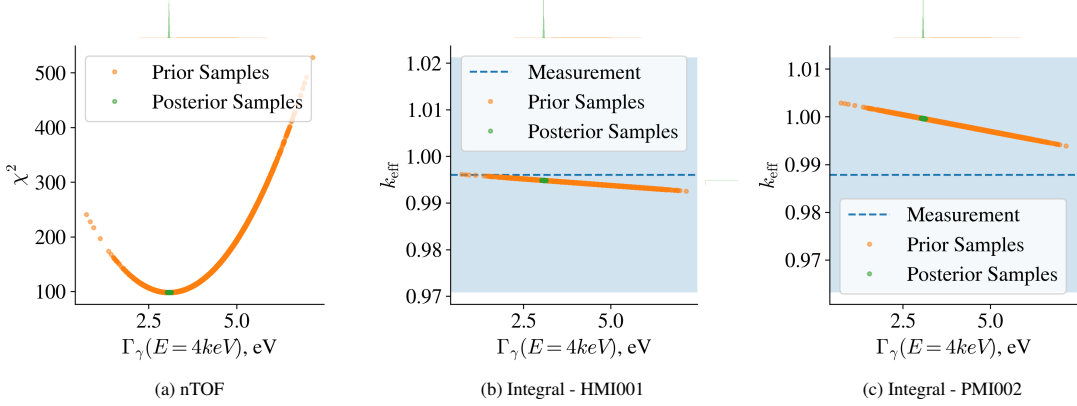


Figure 5: Scatter plots for Case 5 (Independent assumption).

of fully independent microscopic data points is used, such as in case 7 or also in Figure 5. Here the posterior seems to be confident in the prediction of Γ_γ with a posterior uncertainty of 2%.

In Figure 4, corresponding to case 4 is depicted. Here the two integral experiments PMI-002 and HMI-001 as well as the microscopic dataset (regarded as fully correlated) from Pérez-Maroto are included. The posterior prediction of k_{eff} moves away from the calculated integral response for PMI-002, but remains well within the uncertainty bounds imposed by experimental and other nuclear data sources. It appears that the included integral experiments contribute negligibly to the uncertainty reduction in the Γ_γ parameter at 4 keV. In order to be able to include integral experiments into this mix, several things are needed. First, the nuclear data uncertainties of other sources should be kept to a minimum, either by experimental design, or by reducing them using data assimilation with integral experiments that are sensitive to the most important other nuclear data uncertainties. Nevertheless, it seems criticality experiments are not sufficiently sensitive to the Γ_γ -width of ^{53}Cr at 4 keV. A possible route to increase the sensitivity is to design experiments specifically sensitive to this energy range, e.g. pile-oscillation experiments with a significant portion of the spectrum in this energy range. On the other hand, nuclides which are more important for k_{eff} , such as $^{238}\text{U} / ^{235}\text{U}$ or ^{239}Pu might be more suitable candidates for testing as a much larger suite of highly sensitive integral experiments are available.

Finally, we simulate a hypothetical scenario with highly sensitive integral experiments (experimental uncertainty reduced to 10 pcm and other nuclear data uncertainties neglected). As seen in Figure 6, under these ideal and unrealistic conditions, integral experiments provide significant guidance to the posterior. Although we know the integral experiments are subjected to larger uncertainties of other nuclides, it shows that when experiments with a lower uncertainty in comparison to the sensitivity are used, they can be combined with microscopic experiments under the conservative assumption that microscopic data points behave as one.

5. Conclusions and Future Work

In this work, a Bayesian Optimization framework was implemented to infer nuclear data parameters by consolidating microscopic and integral experiments. The methodology coupled SAMMY and SERPENT with Gaussian Process surrogates and an MCMC sampler, allowing for more efficient exploration of the posterior distribution.

The case study on ^{53}Cr highlighted the critical challenge of weighting different data sources. We demonstrated that the assumption regarding correlations in microscopic data fundamentally alters the posterior. Treating microscopic points as independent results in an overconfident reduction of uncertainty in which integral experiments become negligible. On the other side, when microscopic data is treated as fully correlated (per experiment) and uncertainties for other nuclides are also included, the criticality experiments currently available for ^{53}Cr provide negligible information gain. They are dominated by the uncertainties due to fissile nuclides.

The results indicate that for integral experiments to be valuable in this framework, either the experiments must be chosen such that the parameter to infer is sufficiently sensitive in comparison to other nuclear data, or the uncertainties of other nuclear data must be significantly reduced using a-priori data assimilation techniques.

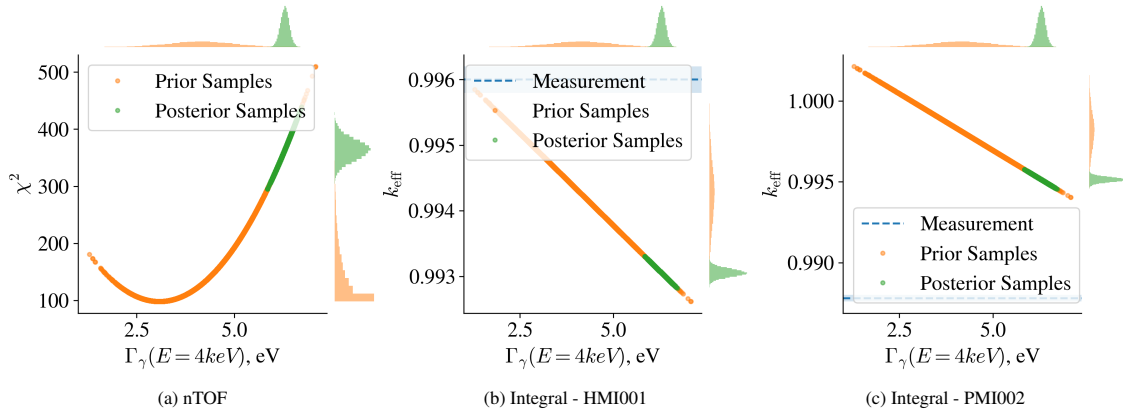


Figure 6: Scatter plots for the hypothetical high-sensitivity scenario.

Future work should be devoted to including a realistic experimental covariance matrix to assess the validity of the assumptions regarding independent / fully correlated data samples. Second, since the case study on ^{53}Cr did not yield significant results, the framework could be applied to a realistic scenario involving for example ^{238}U , where many highly sensitive integral experiments are available. Some points that still should be addressed include implementing correlations between experiments and including the GP prediction uncertainty in the loglikelihood of the microscopic experiment. Although the latter is not expected to influence the results since SAMMY is deterministic, therefore the prediction uncertainty attributed to the GP response is negligible.

6. Acknowledgments

The authors gratefully acknowledge the financial support of the Fonds de la Recherche Scientifique (F.R.S.-FNRS) and the ENEN2plus project. The ENEN2plus project has received funding from the Euratom research and training programme 2021-2025 under grant agreement No 101061677.

References

- [1] N. M. Larson, Updated User's Guide for Sammy: Multilevel R-Matrix Fits to Neutron Data Using Bayes' Equations. doi:10.2172/941054.
URL <http://www.osti.gov/servlets/purl/941054-BqQIHy/>
- [2] J. Leppänen, M. Pusa, T. Viitanen, V. Valtavirta, T. Kaltiaisenaho, The Serpent Monte Carlo code: Status, development and applications in 2013, Annals of Nuclear Energy 82 (2015) 142–150. doi:10.1016/j.anucene.2014.08.024.
- [3] A. Hoefer, O. Buss, J. C. Neuber, Limitations of the Generalized Linear Least Squares Methodology for Bias Estimation in Criticality Safety Analysis.
- [4] D. Rochman, E. Bauge, A. Vasiliev, H. Ferroukhi, S. Pelloni, A. J. Koning, J. Ch. Sublet, Monte Carlo nuclear data adjustment via integral information, The European Physical Journal Plus 133 (12) (2018) 537. doi:10.1140/epjp/i2018-12361-x.
- [5] A. Hoefer, O. Buss, M. Hennebach, M. Schmid, D. Porsch, MOCABA: A general Monte Carlo–Bayes procedure for improved predictions of integral functions of nuclear data, Annals of Nuclear Energy 77 (2015) 514–521. doi:10.1016/j.anucene.2014.11.038.
- [6] D. Foreman-Mackey, D. W. Hogg, D. Lang, J. Goodman, emcee: The mcmc hammer, Publications of the Astronomical Society of the Pacific 125 (925) (2013) 306–312. doi:10.1086/670067.
URL <http://dx.doi.org/10.1086/670067>

- 204 [7] M. Aufiero, A. Bidaud, M. Hursin, J. Leppänen, G. Palmiotti, S. Pelloni, P. Rubiolo, A collision history-based
205 approach to sensitivity/perturbation calculations in the continuous energy Monte Carlo code SERPENT, Annals
206 of Nuclear Energy 85 (2015) 245–258. doi:10.1016/j.anucene.2015.05.008.
- 207 [8] L. Fiorito, J. Dyrda, M. Fleming, JEFF-3.3 covariance application to ICSBEP using SANDY and NDAST, EPJ
208 Web of Conferences 211 (2019) 07003. doi:10.1051/epjconf/201921107003.
- 209 [9] D. W. Muir, R. M. Boicourt, A. C. Kahler, J. L. Conlin, W. Haeck, The NJOY Nuclear Data Processing System,
210 Version 2016.
- 211 [10] B. L. Broadhead, B. T. Rearden, C. M. Hopper, J. J. Wagschal, C. V. Parks, Sensitivity- and Uncertainty-Based
212 Criticality Safety Validation Techniques, Nuclear Science and Engineering 146 (3) (2004) 340–366. doi:10.
213 13182/NSE03-2.
- 214 [11] A. Trkov, O. Cabellos, R. Capote, Sensitivity of selected benchmarks to Cr-53 and Cr-50 capture.
- 215 [12] K. H. Guber, P. E. Koehler, D. E. Wiarda, J. A. Harvey, Neutron Cross-Section Measurements on Structural
216 Materials at ORELA, Journal of the Korean Physical Society 59 (2(3)) (2011) 1685–1688. doi:10.3938/
217 jkps.59.1685.
- 218 [13] R. Stieglitz, R. Hockenbury, R. Block, kev neutron capture and transmission measurements on 50cr, 52cr, 53cr,
219 54cr, 60ni and v, Nuclear Physics A 163 (2) (1971) 592–624.
- 220 [14] International Criticality Safety Benchmark Evaluation Project (ICSBEP), International Handbook of Evaluated
221 Criticality Safety Benchmark Experiments, OECD Nuclear Energy Agency (NEA), 2024.